Journal of Atmospheric and Solar–Terrestrial Physics 247 (2023) 106079

Contents lists available at ScienceDirect

Journal of Atmospheric and Solar-Terrestrial Physics

journal homepage: www.elsevier.com/locate/jastp

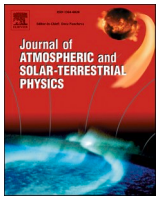

# Geoinduced currents on Karelian-Kola power line and finnish gas pipeline on september, 12–13 2017

P.V. Setsko [a,*], I.V. Despirak [a], Ya.A. Sakharov [a], A.A. Lubchich [a], V.A. Bilin [a], V.N. Selivanov [b]

[a] Polar Geophysical Institute, Apatity, Russia
[b] Northern Energetic Research Center, Kola Science Centre RAS, Apatity, Russia

ARTICLE INFO

Handling Editor: Dora Pancheva

*Keywords:*
Solar wind
Geoinduced currents
Substorm
Westward electrojet
Geomagnetic pulsations

ABSTRACT

Geomagnetic activity and occurrence of large values of geoinduced currents (GICs) during a moderate magnetic storm (SYM/H ~ −65 nT) on September, 12–13 2017 have been studied. Two intense substorms (AL ~600 nT and ~1200 nT) were observed within the period of this magnetic storm. Amplification and motion of electrojets during substorms is known to be one of the important sources of GIC value increase in the auroral zone. The fine spatial temporal structure of westward electrojet has been analyzed using the latitudinal profiles of the IMAGE network and the equivalent currents of the MIRACLE system data. GICs activity were monitored by EURISGIC from Russian stations Vykhodnoy (VKH) and Revda (RVD) in the North-West of Russia (eurisgic.ru) and Mäntsälä station (MAN) in South Finland. The data from these stations are convenient to track GIC from ~60° to ~69° geographical latitudes. It has been shown that the increase in GIC amplitudes at different latitudes was associated with the poleward movement of the westward electrojet during the expansion phase of the substorm. Besides, it has been found that the source of the GICs at the recovery phase of the second substorm appeared to be a short pulse of Pc5 pulsations and the amplitudes of GICs were comparable with substorms one. It is also shown that the increase in GIC amplitude are in good agreement with the increase in the Wp- and IL-geomagnetic indices used for global and local control over the substorm appearance.

## 1. Introduction

Solar wind high speed streams, fast forward shocks, coronal mass ejections (CME) cause rapid changes in geomagnetic field, which, in turn, leads to an increase of intense low frequency currents, the so-called geomagnetically induced currents (GICs), at ground based technological networks, such as power lines, gas pipelines and railways (Viljanen et al., 2006b; Pulkkinen et al., 2005; Lakhina et al., 2020). GICs, the last element in the Sun-Solar wind-magnetosphere-ionoshpere-Earth system, negatively affect the operation of technological networks and can cause their failure (Tsurutani and Hajra, 2021). For this reason, the excitation of GICs in power transmission lines is monitored in many countries located in both high and middle geomagnetic latitudes (e.g. Kelly et al., 2017; Mac Manus et al., 2017; Clilverd et al., 2021; Watari et al., 2021).

In the North-West of Russia, Polar Geophysical Institute together with Northern Energetic Research Center built a system, called EURISGIC, to monitor such currents in the autotransformers neutral line in the existing Karelian-Kola power transmission line (Sakharov et al., 2007, 2016, 2019). This power line is located at geographical (geomagnetic) latitudes from ~60° to ~69° (56.6° to 65.5°) directed from south to north. Note that this location corresponds to auroral latitudes where substorm disturbances are usually observed.

It is known that substorms are connected with strong magnetic disturbances observed within the auroral oval (Akasofu, 1964, 2017). Depending on space weather conditions, the oval location can be classified as contracted, normal, or expanded (Lui et al., 1973). During strong magnetic activity a substorm can be observed within a large latitude area from low to very high latitudes, within expanded oval, these events are called « expanded » or « high-latitude » substorms (e.g., Loomer and Gupta, 1980; Kleimenova et al., 2012; Despirak et al., 2018). At the auroral latitudes substorms are one of the major causes of large GIC (Viljanen et al., 2006a).

Recently it has been confirmed that strong disturbances of the westward electrojet during expansion phase of substorm is one of the reason for the GICs growth (Vorobjev et al., 2018; Kozyreva et al., 2020; Tsurutani and Hajra, 2021; Despirak et al., 2022a). The study made by

* Corresponding author.
*E-mail addresses:* setsko@pgia.ru (P.V. Setsko), despirak@gmail.com (I.V. Despirak), sakharov@pgia.ru (Ya.A. Sakharov), lubchich@pgia.ru (A.A. Lubchich), bilinvlad@gmail.com (V.A. Bilin), v.selivanov@ksc.ru (V.N. Selivanov).

https://doi.org/10.1016/j.jastp.2023.106079
Received 30 December 2022; Received in revised form 17 April 2023; Accepted 7 May 2023
Available online 8 May 2023

Vorobjev et al. (2018) showed that GIC intensity significantly increases with the growth of substorm activity and peaks when the equatorial boundary of auroral oval precipitations is located by ~1° of latitude south of the GIC registration.

In addition, the study of intense GICs (>30 A) over a 20-year period (1999–2019) at Mäntsälä station, Finland (~60.6° geographical latitude) was made by Tsurutani and Hajra (2021). They discovered that the increase of GICs values is most frequently associated with the gain of auroral electrojets during supersubstorms (SML < −2500 nT) and intense substorms (−2500 nT < SML <−2000 nT). The relationship between GICs and supersubstorm (SSS) development was studied in our previous work (Despirak et al., 2022b) where intense GICs during two supersubstorms on September 7–8, 2017 were analyzed. We also studied several complex cases of GIC occurrence during substorms observed during the magnetic storms (Despirak et al., 2022a).

The fact that we have the opportunity to use the meridional chain of the GIC registration network (eurisgic.ru) and the chain of IMAGE magnetometers almost parallel to it (~10° to the west) allows us to trace the fine spatial-temporal structure of the substorm poleward propagation and the large values of GIC during the event. When studying and modeling GIC, it is also necessary to take into account that substorm activity is associated not only with an increase in the intensity of a large-scale westward azimuth electrojet (in the west-east direction), but also has other large meridional manifestations (in the south-north direction), such as poleward movement of the westward electrojet (Kisabeth and Rostoker, 1974; Pudovkin et al., 1995), that occurs in "jumps" to the pole during the substorm expansion phase (Wiens and Rostoker, 1975. In addition, there may be several intensifications in the substorm expansion phase (Sergeev and Yahnin 1979; Yahnin et al., 1983), which is connected with multiple onsets of substorm. In such cases several successive negative bays were registered at ground based magnetic station and such phenomena are associated with several injections of accelerated particles in the magnetosphere (multiple onsets) as was observed, for example, during the substorms that occurred at ~06 UT on March 28, 2010 (Yao et al., 2017) and at ~18 UT on March 17, 2013 (Despirak et al., 2022a).

Despite the fact that an important source of GIC in the auroral zone is intensification and motion of electrojets, there are other reasons for GIC occurrence, i.e. impulses of solar wind dynamic pressure, magnetic pulsations, omega structures in auroras, etc. (Oliveira and Ngwira, 2017; Kozyreva et al., 2020; Apatenkov et al., 2020). Kozyreva et al. (2020) showed that Ps6 and Pc5 pulsations as well as isolated nightside magnetic impulsive events (MIE) are capable to induce noticeable GICs up to ~20 A which were registered at the Vykhodnoy station on the Kola Peninsula.

This work is considering the event on September 12–13 which is associated with the development of a moderate magnetic storm. It should be noted that September of 2017 was an extremely active space weather period with multiple events leading to varying impacts on the Earth's magnetosphere. There were registered some successive solar wind types which sometimes overlapped: interplanetary coronal mass ejections (ICMEs), magnetic clouds (MCs), sheaths, corotating interaction regions (CIRs), high-speed streams (HSSs), fast shocks, etc. This complex solar wind structures caused some magnetic storms, intense substorms, and HILDCAA (High-intensity, long-duration, continuous AE activity) geomagnetic activity in addition to the above two supersubstorms (Hajra et al., 2020).

Solar wind and interplanetary magnetic field (IMF) parameters for the event – from 14:00 UT on September 12 to 10:00 UT on September 13 – are given in Fig. 1. The figure shows from top to bottom: the magnitude ($B_T$) of the interplanetary magnetic field (IMF); the Y- and Z-component of the IMF ($B_Z$); the flow speed ($V$), the density (N), temperature (T), and dynamic pressure ($P$) of solar wind, and the geomagnetic indices $AL$ and $SYM/H$. It is seen that a fast shock (IS) occurred at ~19:55 UT on September 12. The moment of IS registration is marked by the red vertical line and inscription IS. Then from ~20 UT on

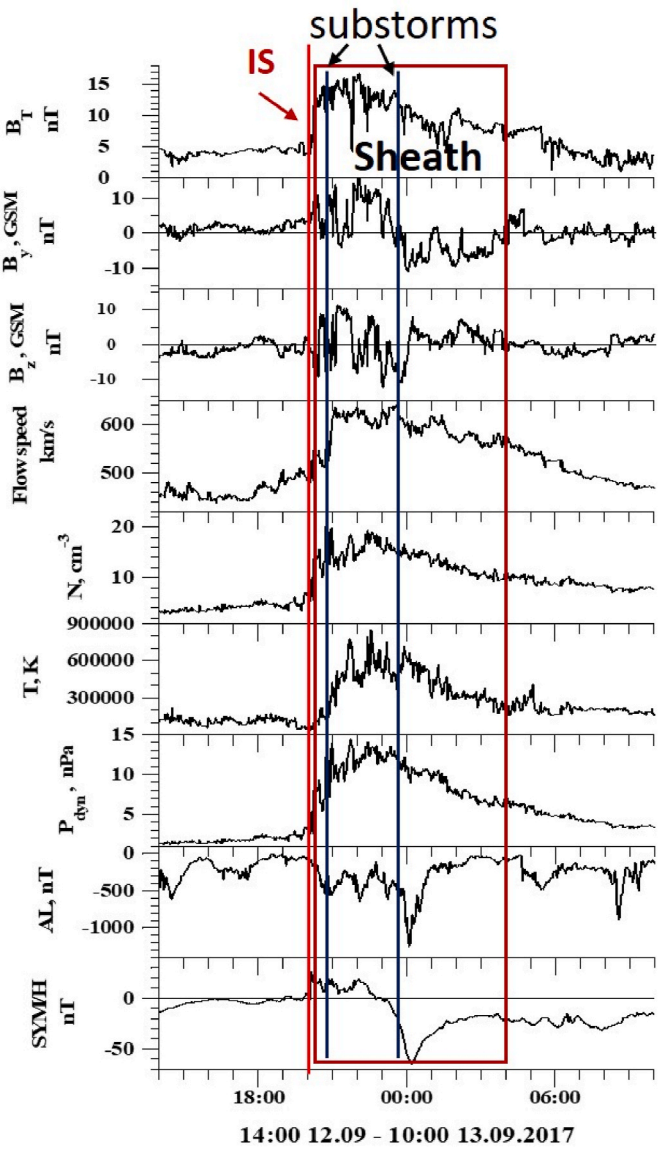


**Fig. 1.** Solar wind and interplanetary magnetic field (IMF) parameters from 14:00 UT on 12 September to 10 UT September 13, 2017. From top to bottom: the magnitude (BT) of the interplanetary magnetic field (IMF); the Y- and Z-component of the IMF (BZ); the flow speed (V), the density (N), temperature (T), and dynamic pressure (P) of solar wind, and the geomagnetic indices AL and SYM/H.

September 12 the region with increasing dynamic pressure (P dyn) and solar wind density (N) was registered, it was so-called sheath region. The boundaries of the sheaths, from ~20 UT on September 12 to ~04 UT on September 13, are marked by the red rectangle and inscription Sheath. Note that sheath is the region of compressed plasma at the front of MC, different types of solar wind were determined from the catalog of large-scale solar wind types (Yermolaev et al., 2009). It is seen that some discrete southward Bz periods were observed (~−10 nT). These periods led to a moderate magnetic storm (SYM/H ~ −65 nT at ~00:10 UT) on September 13. During this storm there were two intense substorms with maximum AL ~ −600 nT and ~ −1200 nT (SML ~ 1070 nT and ~1540 nT, not shown), respectively, which are marked as blue lines and inscription substorms. We determined onsets of substorms by IMAGE magnetometers data, by a sharp onset of negative bay on the most equatorial station on the meridional chain. However, Fig. 1 presents the moments of substorm onsets rather schematically since the time interval is quite long. During these two substorms there were registered intense

GICs on Karelian-Kola power line (Vykhodnoy and Revda stations) and on the Finland gas pipeline near Mäntsälä, which will be considered in more detail below.

## 2. Data

The spatial distribution of the substorm electrojets was determined using the magnetometers of the IMAGE (http://space.fmi.fi/image/) and SuperMAG (http://supermag.jhuapl.edu/) networks. To study the spatial distribution of magnetic disturbances on the IMAGE profile, instant maps of the distribution of ionospheric equivalent electric currents MIRACLE (https://space.fmi.fi/MIRACLE/) have been analyzed (Viljanen and Häkkinen, 1997). The MIRACLE system include also all-sky cameras and TomoScand Receiver, but these data not used in current work.

The onset of substorms have been determined by IMAGE magnetometers data by a sharp onset of negative bay on the most equatorial station on the meridional chain PPN-NAL; the onset of intensification of substorm have been determined similarly for each intensification.

To analyze the GICs we took the data from two recording systems: 1) GIC registration system EURISGIC (http://eurisgic.ru/) located in the North-West of Russia in the auroral zone on the power line directed south-north (Sakharov et al., 2007, 2016, 2019). This system used a current detection sensor mounted on the neutral line of an autotransformer to measure the GIC. Positive values mean GIC going into the ground 2) GIC registration system in Finland on gas pipeline directed east-west station near Mäntsälä in the subauroral zone (https://space.fmi.fi/gic/index.php). Fig. 2 shows the scheme of EURISGIC recording stations and Mäntsälä station (red and white dots with data and no data at selected time, respectively), as well as part of the PPN-NAL meridional chain of IMAGE magnetometers (black dots). In accordance with the geographic location of the networks and Faraday's law of induction, and also neglecting geology and branches of networks, increase of the GIC at VKH and RVD stations will be driven by rapid change in the Y-component of the magnetic field, while at MAN station – X-component. For visual demonstration that assumption we use corresponding magnetic field component of IMAGE station nearest to GIC recording station (black lines on Figs. 3c–5c). On Fig. 2 these stations are marked as black dots with orange border: for Vykhodnoy (VKH) – Masi (MAS), for Revda (RVD) – Muonio (MUO) and for Mäntsälä (MAN) – Nurmijärvi (NUR). A complete list of PPN-NAL chain with geographic and geomagnetic coordinates of the stations is presented in Table 1. Table 1 contains the coordinates of used GIC stations as well (in bold).

The global spatial distribution of substorms was also determined from the maps of magnetic field vectors obtained from observations on the SuperMAG network (Gjerloev, 2009; Newell and Gjerloev, 2011).

The IL- and SML-indexes are also taken from IMAGE and SuperMAG networks, correspondingly. Note that the IL index shows the variation of the magnetic field at the selected IMAGE stations, that is, in essence, it is similar to the AL index which is associated with the auroral electrojet.

We also used the Wp (wave and planetary) index which is related to the power of the Pi2 pulsation wave at low latitudes and associated with the substorm onset. Wp-index is calculated from the data of 11 ground-based magnetic stations located between 20° and 50° MLAT around the North Pole (Nosé et al., 2012).

The solar wind and IMF parameters are taken from OMNI database ftp://ftp.iki.rssi.ru/omni/ and the catalog of large-scale solar wind types ftp://ftp.iki.rssi.ru/pub/omni/catalog

## 3. Results

The general scheme of magnetic disturbances and GICs registrations from 18 UT to 04 UT for the September 12–13 event is shown on Fig. 3. The left panel of the Figure shows the variations of X component of IMAGE magnetometers from SUW to NAL (PPN-NAL chain) (a), the right top panel – the SuperMAG maps of magnetic field vectors (b), the right bottom panel – GICs data (red lines) with corresponding magnetic component of nearest IMAGE station (black lines) and geomagnetic indexes Wp and IL (blue lines) (c). For station MAS (close to VKH) and MUO (close to RVD) presented Y-component of magnetic field, for station NUR (close to MAN) – X-component of magnetic field. The geographical latitudes of stations (GLAT) are used. In figure (3a and 3c) three periods of different magnetic disturbances and large values of GIC from 20 to 23 UT, from 23 to 01 UT and from 01 to 02:30 UT are marked by horizontal bars and dashed lines. The first two blue bars show the periods of two substorms mentioned in Introduction. The third orange bar shows the period of Pc5 pulsations. SuperMAG polar maps correspond to maximum of magnetic disturbances for these three events in time. Let's consider each event separately.

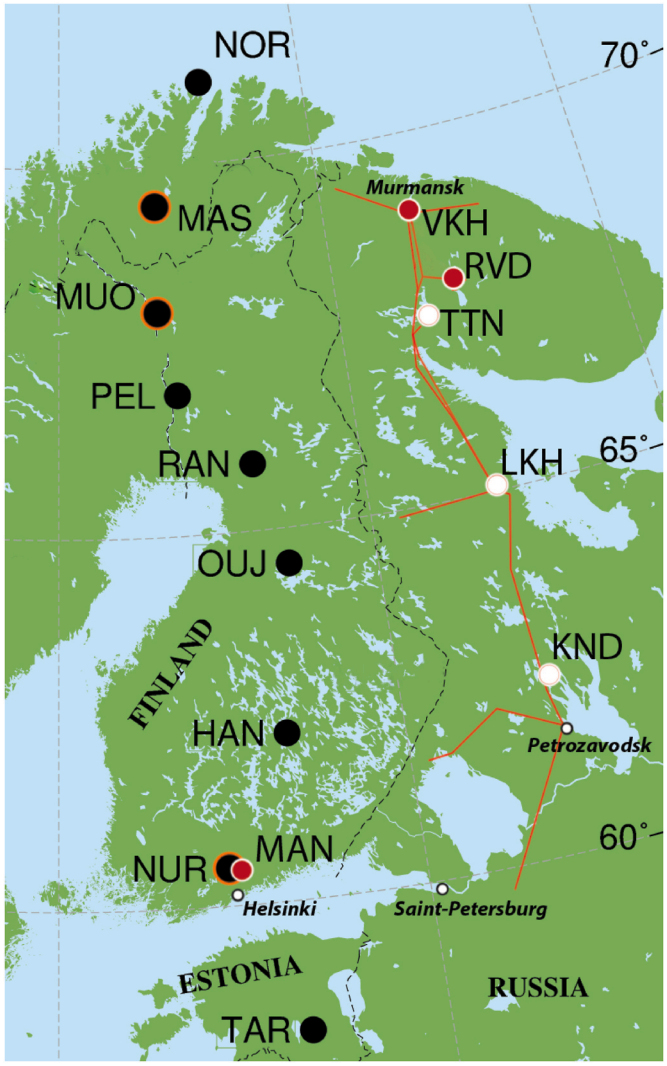


**Fig. 2.** The geographic map of GICs recording stations and nearby observatories for measuring geomagnetic variations both in the North-West of Russia and in Finland. Black dots – IMAGE magnetometer stations, red dots with a white border – used in work GIC registration stations, black dots with an orange border – the magnetometer stations closest to GIC registration stations, white dots – GIC registration stations with no data at selected time. (For interpretation of the references to color in this figure legend, the reader is referred to the Web version of this article.)

### 3.1. First substorms

Fig. 4 shows the first event for study from 20 to 23 UT on September

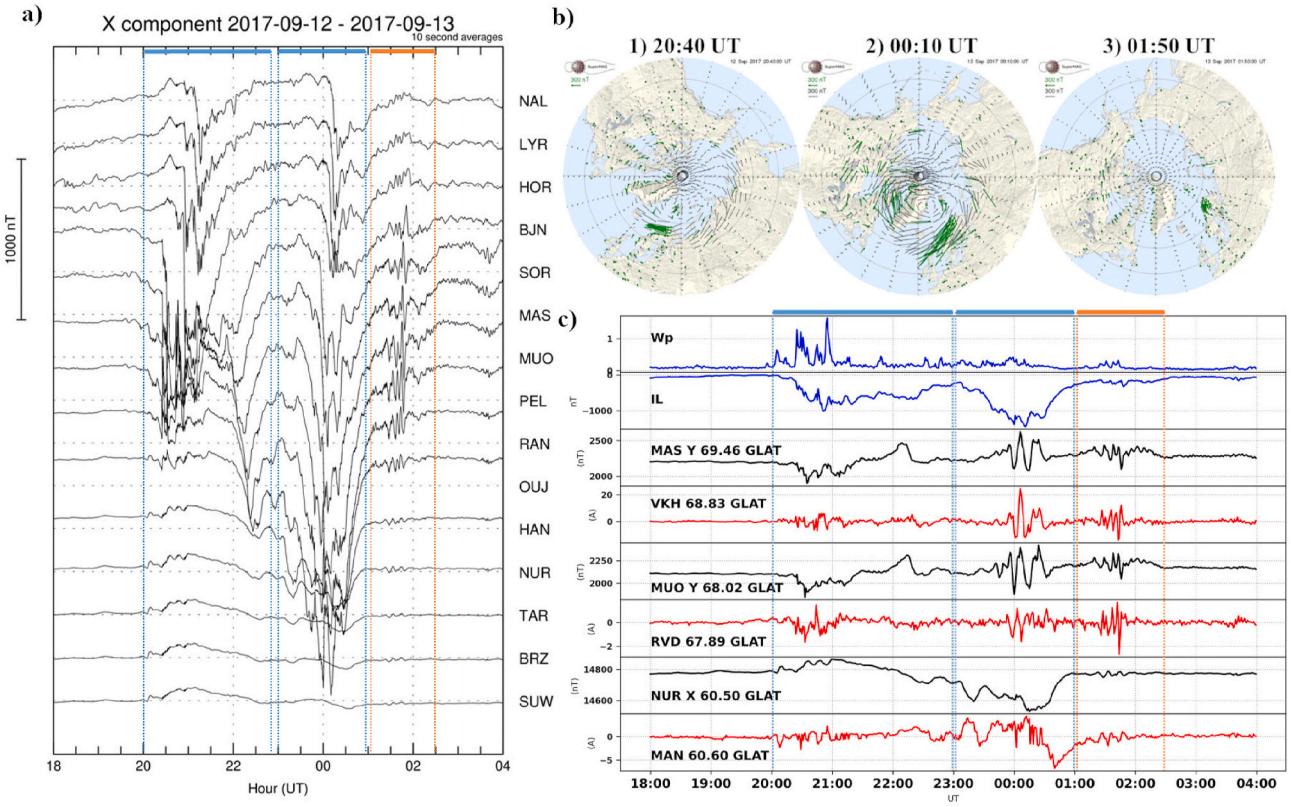


**Fig. 3.** The magnetic disturbances and GICs registrations from 18 UT to 04 UT 12–13 September 2017. Blue and orange bars with dotted lines mark three different events during this time. a) the variations of X component of IMAGE magnetometers from SUW to NAL (PPN-NAL chain); b) the SuperMAG maps of magnetic field vectors during maximum disturbance at each of the three events; c) geomagnetic indexes Wp and IL (blue lines) and GICs data (red lines) with Y-component of magnetic field at MAS and MUO, and X-component at NUR (black lines). (For interpretation of the references to color in this figure legend, the reader is referred to the Web version of this article.)

12, 2017. The format of Fig. 4 is similar to that of Fig. 3, but a map of equivalent currents calculated according to the MIRACLE system replaces the SuperMAG maps of magnetic vectors. The left panel shows the X component of PPN-NAL chain of IMAGE magnetometers from 20 UT to 23 UT (a). The maps of latitudinal profile of the westward and eastward electrojet from 19:30 UT to 23:00 UT are located on the upper right panel (b). Below this panel, there are GICs data with corresponding magnetic component of the nearest IMAGE station and geomagnetic indexes for the same time (c).

The first substorm began at ~20:20 UT on September, 12 and consisted of 4 intensifications which are marked as blue dotted lines on Fig. 4a. The onset of the first intensification was manifested by a sharp onset of negative bay observed at the more equatorial station. As seen, the first intensification began at 20:25 UT on MUO station, it propagated rapidly to SOR station and did not propagate higher. As well as the second intensification which began at 20:45 UT. The third and fourth intensifications (~20:55 UT and ~21:10 UT respectively) started at auroral latitudes and, unlike the first two, rapidly propagated to the LYR and NAL stations. At this time, as can be seen from MIRACLE data on Fig. 4b, the westward electrojet moved from 66° N to 78° N on expansion phase of substorm, and we can see the same intensifications at the corresponding time in westward electrojet profile which is marked in blue in Fig. 4b.

As seen from SuperMAG polar map at 20:40 UT (Fig. 3b) the main disturbances during this substorm were in the premidnight sector under the Kola Peninsula. And that is where our GICs registration stations are located. Fig. 4c shows GICs data (red lines) and the disturbances in these data correspond to substorm intensifications. The first two are seen at about 20:30 UT and about 20:45 UT at all three used stations: VKH (up to 6 A), RVD (up to 1.5 A) and MAN (up to 2 A), the other two at about 20:50 UT and about 21:10 UT are seen only at the VKH station (up to 5 A). This correspond to their geographical location relative to electrojet movement to the pole. Fig. 4c shows the peaks in the Wp index (upper blue line): the highest peak appeared when the most intense GICs were registered and a small one occurred before the onset of the substorm. The small one coincides with the disturbance only at MAN station. Thus, the dependence of the increase of GICs on the substorm spatial temporal structure can be clearly seen.

### 3.2. Second substorms

The blue bars on Fig. 5 show the next period for study, i.e. occurrence of large values of GICs during the second substorm. The format of Fig. 5 is similar to that of Fig. 4. On Fig. 5 the X-components of PPN-NAL chain of IMAGE magnetometers from 23 UT 12 September to 03 UT 13 September are located on the left panel (a). The latitudinal profile of the westward and eastward electrojets from 23:00 UT September 12 to 02:30 UT September 13 are located on the upper right panel (b). Below the GICs data with corresponding magnetic component of the nearest IMAGE station and Wp- and IL-indexes at the same time (c) are given.

The second substorm began at ~23:20 UT on September 12 at OUJ station and propagated to NAL station where the disturbance started at ~00:10UT on September 13 (the onset of substorm was determined by a sharp onset of the negative bay observed at the more equatorial station). As seen from MIRACLE data in Fig. 5b, the westward electrojet (blue color) started to develop on 63°–66° N geographical latitudes and propagated to the north after midnight up to 73°N with small jumps up to 80°N and enhancements on 65°N during the expansion phase of substorm. According to SuperMAG polar map at 00:10 UT on September 13 (Fig. 3b), the disturbances were in the premidnight and

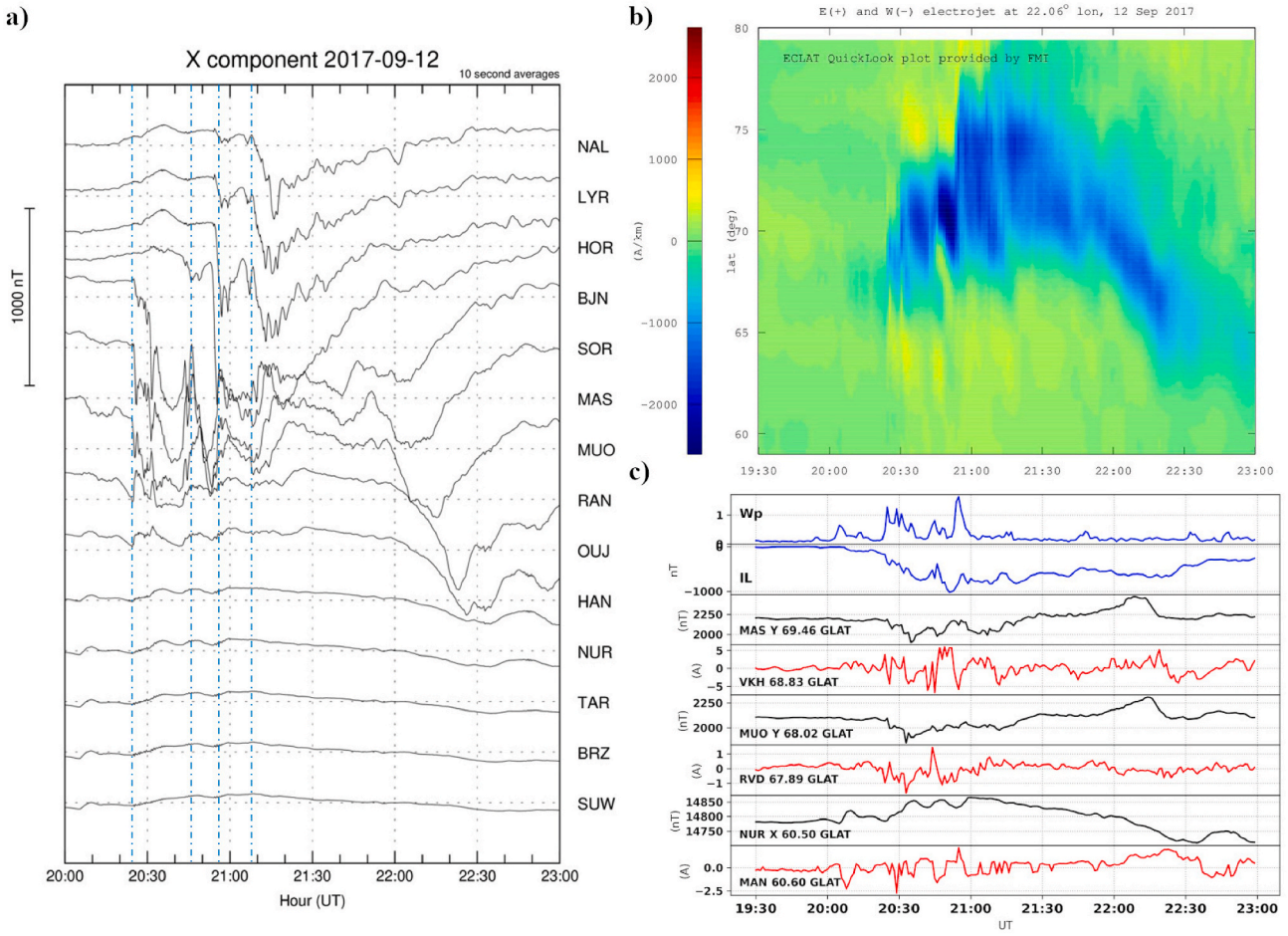


**Fig. 4.** The first substorm on September 12, 2017; a) the X component of PPN-NAL chain of IMAGE magnetometers from 20 UT to 23 UT. Blue dashed lines correspond to 4 substorm intensifications; b) latitudinal profile of the westward (blue) and eastward (yellow) electrojets of MIRACLE system from 19:30 UT to 23:00 UT; c) geomagnetic indexes (blue lines) and GICs data (red lines) with corresponding magnetic component of nearest IMAGE station (black lines) from 19:30 UT to 23:00 UT. (For interpretation of the references to color in this figure legend, the reader is referred to the Web version of this article.)

postmindnight sectors under East Canada, Greenland and Scandinavia. The GICs registration stations were in after midnight sector and the disturbances in GICs data profiles are presented in Fig. 5c. The most intense current (~22 A) occurred at VKH station after midnight at ~ 00:10 UT during the expansion phase of the substorm, when the westward electrojet rushed toward the pole and the magnetic storm had its minimum in SYM/H. There are good accordance between the variations of Y-component values at the MAS and MUO magnetometers and variations of GIC values at VKH and RVD stations. At MAN and NUR stations the accordance looks worse because the substorm developed at higher latitudes. The highest peak in Wp index was regiserd at ~00:10 UT during the maximum of the expansion phase of the substorm. Note that this index also had smaller peaks before the onset of the second substorm that coincided only with GICs data at the MAN station, while no disturbances occurred in the GICs profiles at VKH and RVD stations. The same situation was observed in the previous case during the first substorm and this fact can be connected with Wp calculation approach (Nosé et al., 2012). The index is calculated from measurements taken at equatorial stations, therefore, it is more sensitive to disturbances occurred at mid latitudes than at high latitudes.

There was also one more significant GIC value (~7 A) during this substorm at Mantsala at 00:40 UT which is not associated with the movement of the westward electrojet to the pole. However, as can be seen from the variation of the IL index, at this time there was a change in the intensity of the electrojet associated with the recovery phase of the substorm. We suppose that such slow changes in the strength of the current flowing in the direction from east to west might also lead to an increase in the GIC on the Mantsala pipeline.

So, in the second event the dependence of the increase of GICs on the spatial temporal development of the substorm is manifested: the westward expansion of the electrojet corresponds to the peaks in the GICs profiles from MAN to VKH.

### 3.3. Magnetic pulsation Pc5

The orange bars in Fig. 5 show the last period for study – the occurrence of significant GICs values during the period from ~01:00 UT to ~02:30 UT on September 13, 2017. According to IMAGE data periodical disturbances (pulsations) after 01:20UT can be seen from OUJ to NAL stations (Fig. 5a), which corresponds to frequency of ~3–8 mHz (the period of these pulsations was ~ 2–5 min), i.e. these pulsations fit to Pc5 pulsations.

Note that monochromatic Pc5 pulsations is a typical event for early morning hours during the recovery phase of a substorm (Kozyreva et al., 2020) and these pulsations are observed precisely at the recovery phase of the second substorm. As seen from Fig. 5c during these pulsations there were registered significant GICs at VKH station up to 16 A and RVD station up to 5 A. There good accordance is seen between pulsations in the Y-component at the MAS and MUO magnetometers and GIC variations at VHD and RVD stations. Since pulsations are intense only at OUJ station and higher, significant GICs at Mäntsälä station were not registered. Thus, as in other works (Yagova et al., 2021), Pc5 pulsations

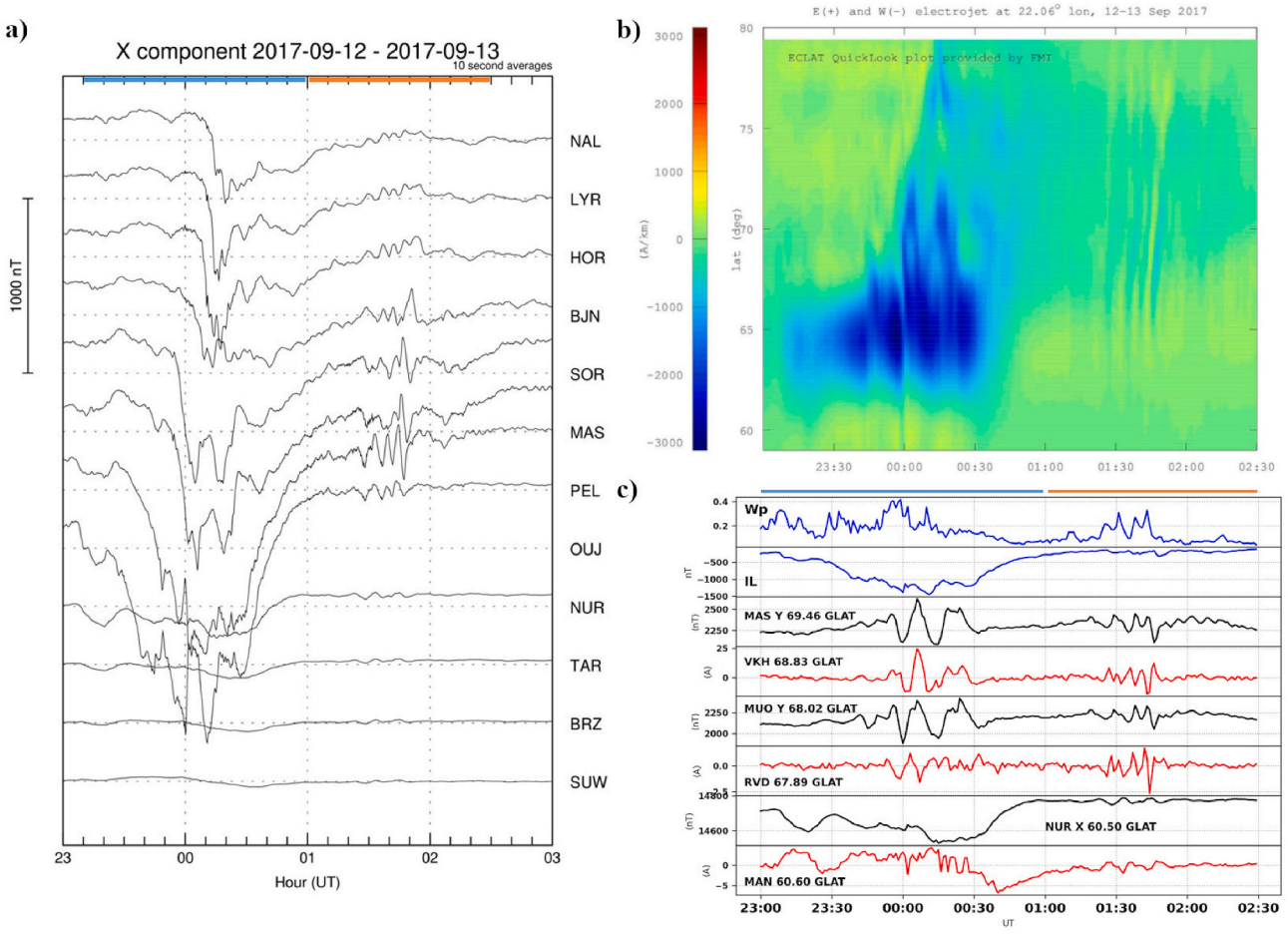


**Fig. 5.** The period of a second substorm marked by blue bar and the period of a Pc5 pulsations marked by orange bar; the same format as on Fig. 4 from 23 UT 12 September to 03 UT 13 September. (For interpretation of the references to color in this figure legend, the reader is referred to the Web version of this article.)

**Table 1**
A list of PPN-NAL meridional chain of IMAGE magnetometers and used GIC stations (in bold) with geographic and geomagnetic coordinates. The magnetometer stations closest to GIC stations are underline and in italic.

| Station code | Station name | GGLAT (deg) | GGLON (deg) | CGMLAT (deg) | CGMLON (deg) |
|---|---|---|---|---|---|
| NAL | Ny Ålesund | 78.92 | 11.95 | 75.25 | 112.08 |
| LYR | Longyearbyen | 78.20 | 15.82 | 75.12 | 113.00 |
| HOR | Hornsund | 77.00 | 15.60 | 74.13 | 109.59 |
| BJN | Bear Island | 74.50 | 19.20 | 71.45 | 108.07 |
| SOR | Sørøya | 70.54 | 22.22 | 67.34 | 106.17 |
| *MAS* | *Masi* | *69.46* | *23.70* | *66.18* | *106.42* |
| **VKH** | **Vykhodnoy** | **68.83** | **33.08** | **65.53** | **112.73** |
| *MUO* | *Muonio* | *68.02* | *23.53* | *64.72* | *105.22* |
| **RVD** | **Revda** | **67.89** | **34.16** | **64.65** | **112.87** |
| PEL | Pello | 66.90 | 24.08 | 63.55 | 104.92 |
| RAN | Ranua | 65.90 | 26.41 | 62.09 | 105.91 |
| OUJ | Oulujärvi | 64.52 | 27.23 | 60.99 | 106.14 |
| HAN | Hankasalmi | 62.25 | 26.60 | 58.69 | 104.54 |
| **MAN** | **Mäntsälä** | **60.60** | **25.20** | **57.29** | **102.05** |
| *NUR* | *Nurmijärvi* | *60.50* | *24.65* | *56.89* | *102.18* |
| TAR | Tartu | 58.26 | 26.46 | 54.47 | 102.89 |
| BRZ | Birzai | 56.17 | 24.86 | 52.30 | 100.81 |
| SUW | Suwałki | 54.01 | 23.18 | 49.97 | 98.70 |

caused significant GICs in power lines in our case too.

## 4. Discussion

Three events of intensive GICs observations on the latitudinal profile of GICs registration in the North-West of Russia have been analyzed together with the data of GICs registration on the gas pipeline near the Mäntsälä station in Finland. The use of the latitudinal profile of the GIC data made it possible to trace the increasing of the GIC in accordance with the poleward expansion of the substorm and the development of its fine structure. As seen from Fig. 4, time moments of GICs enhancement are well correlated with the moments of four intensifications of the first substorm at ~20:25, ~20:45, ~20:55, ~21:10 UT. Before the onset of the substorm, the strongest GICs were observed mainly at Mäntsälä station; and with the onset of the expansion phase of the substorm (~20:22 UT), small GICs were also observed at the RVD and VKH stations. Further, the strongest GICs at VKH were observed at the moment ~20:50UT when the strong increasing of the westward electrojet and their moving to high-latitudes were registered (Fig. 4b).

Note also that the second substorm developed in a differrent form. This substorm belonged to "high-latitude" (or "expanded") ones since, according to Z-component variations of PPN-NAL chain of IMAGE magnetometers (not shown), the center of the westward electrojet (more intense current) moved from OUJ to LYR. Besides, "high-latitude" ("expanded") substorms are usually registered during high-speed streams (HSS) or sheath region in the solar wind at high values of solar wind velosity (Despirak et al., 2014, 2018). According to the data from MIRACLE system (Fig. 5b), the disturbances began at geographic latitude ~63–64° N and then we see a fast expansion of westward electrojet to the pole to the latitude ~78° N (to the NAL station). It can be seen that the substorm disturbances occurred almost simultaneously at the corresponding latitudes with a small time delay of ~10 min between the onset and the maximum phase of the substorm (from the OUJ

stations to the NAL stations). And at this moment GICs increased almost simultaneously at the corresponding latitudes (from MAN to VHK). The strongest GIC was observed at VKH at ~00:10 UT on September 13, 2017. Thus, it can be seen that the enhancement of GIC at different latitudes is similar to the moving of the westward electrojet during the expansion phase. This result is confirmed by earlier researches that studied other intense substorm events at the same latitudinal profile (Vorobjev et al., 2018; Kozyreva et al., 2020; Despirak et al., 2022a; Setsko et al., 2022). The relationship showed between the increase in the geomagnetic indices IL and Wp and the GICs also indicates the dependence of the GIC enhancement on substorm activity. However, it should be noted that, in general, there is no unambiguous correspondence between these indices and GIC enhancement. We assume that this may be due to the fact that the Wp index is calculated from 11 mid-latitude stations located around the entire globe and shows the onset of substorms at different longitudes. And when studying the magnetic variations of the IL index, it is necessary to take into account not only its strong variations, but also slow changes. Thus, it is good to use these indices for assessing the development of global and local magnetic substorms; they are in good agreement with the increase in the GIC amplitude, but do not always exact fit.

There is also an opinion that an actual driver of GICs is not the auroral electrojet, but isolated or multiple, impulsive, short-lived (~10 min time scale) disturbances embedded in it (Kozyreva et al., 2020). On the one hand, our observations confirm this assumption. As seen on Fig. 4a and b, the expansion phase of substorm consisted of four intensifications, which may be considered as impulses events. On the other hand, it is seen that sometimes there may be observed some intense GIC associated with smooth changes in the strength of the westward electrojet (for example, GIC ~7 A at MAN during the recovery phase of the second substorm).

Strong variations of the magnetic field can be associated not only with the onset of substorms and the moving of electrojets, but Ps6/Pi3 and Pc5 geomagnetic pulsations (Kozyreva et al., 2020; Yagova et al., 2021) and dB/dt spikes of the magnetic field (Schillings et al., 2022). It was shown that rapidly varying electromagnetic fields during these disturbances can induce a signifcant GIC, sometimes up to ~120 A (Viljanen 1998; Apatenkov et al., 2004, 2020). In the considered event on September 13, 2017, a short pulse of Pc5 pulsations which were observed at the recovery phase of the second substorm, caused GICs at Vykhodnoy ~16 A and Revda ~ 5 A. Whereas the GICs during the first substorm are ~6 A (VKH), ~2 A (RVD) and during the second substorm are ~ 22 A (VKH), ~2 A (RVD). So, it is seen that the GICs generated by substorms and by Pc5 pulsations are comparable. This result is consistent with one of the conclusions in the statistical study made by Sakharov et al. (2022). They showed that at auroral latitudes, GICs can be generated by both high-amplitude storm-time Pc5–6/Pi3 pulsations and by non-storm ones with moderate amplitudes (Sakharov et al., 2022).

## 5. Conclusions

Three events of GICs enhancement during a moderate storm on September 12–13, 2017 were connected with an increase and an expansion of the westward electrojet during two substorms and with short bursts of Pc5 pulsations.

1. It was possible to track GICs enhancement along the meridian (from Mäntsälä to Vykhodnoy) according to fine spatial temporal structure of the substorm development for the given events. GICs increase at different latitudes corresponds to the poleward movement on the west electrojet.
2. The most intense GICs (>20 A at VKH station) were recorded during the expansion phase of the midnight intense substorm almost simultaneously at all stations from 57.3 to 65.5 CGMLAT
3. The source of the GICs during the third period was short pulses of Pc5 pulsations at the recovery phase of an intense substorm.
4. The moments of GIC increase coincide with the moments of increase of Wp and IL geomagnetic indexes values that are commonly used for global and local monitoring of substorm development.

## Declaration of competing interest

The authors declare that they have no known competing financial interests or personal relationships that could have appeared to influence the work reported in this paper.

## Data availability

Data will be made available on request.

## Acknowledgements

The authors are grateful to the creators of the OMNI databases (http://cdaweb.gsfc.nasa.gov/cdaweb/istp_public/), the SuperMAG network (http://supermag.jhuapl.edu/), the EURISGIC system (https://eurisgic.ru)(https://eurisgic.org/https://eurisgic.org/), the MIRACLE system (https://space.fmi.fi/MIRACLE/) and the Wp index (https://www.isee.nagoya-u.ac.jp/) for the ability to use them in our work. And also to the Finnish Meteorological Institute for Mäntsälä GIC data, IL-index and IMAGE magnetometers network (https://space.fmi.fi/image/). The work of P.V. Setsko, I.V. Despirak, A.A. Lubchich and V.A. Bilin was supported by the RFBR (№ 20-55-18003 Bulg_a) and National Science Fund of Bulgaria (NSFB) (№ КП-06-Русия/15).

## References

Akasofu, S.-I., 1964. The development of the auroral substorm. Planet. Space Sci. 12 (4), 273–282. https://doi.org/10.1016/0032-0633(64)90151-5.

Akasofu, S.-I., 2017. Where is the magnetic energy for the expansion phase of auroral substorms accumulated? 2. The main body, not the magnetotail. J. Geophys. Res. Space Physics 122, 8479–8487. https://doi.org/10.1002/2016JA023074.

Apatenkov, S.V., Sergeev, V.A., Pirjola, R., Viljanen, A., 2004. Evaluation of the geometry of ionospheric current systems related to rapid geomagnetic variations. Ann. Geophys. 22, 63–72.

Apatenkov, S.V., Pilipenko, V.A., Gordeev, E.I., Viljanen, A., Juusola, L., Belakhovsky, V. B., Sakharov, Ya A., Selivanov, V.N., 2020. Auroral omega bands are a significant cause of large geomagnetically induced currents. Geophys. Res. Lett. 47, e2019GL086677 https://doi.org/10.1029/2019GL086677.

Clilverd, M.A., Rodger, C.J., Freeman, M.P., Brundell, J.B., Mac Manus, D.H., Dalzell, M., Clarke, E., Thomson, A.W.P., Richardson, G.S., MacLeod, F., Frame, I., 2021. Geomagnetically Induced Currents during the 07–08 September 2017 Disturbed Period: a Global Perspective J, vol. 11. Space Weather Space Clim, p. 33. https://doi.org/10.1051/swsc/2021014.

Despirak, I.V., Lyubchich, A.A., Kleimenova, N.G., 2014. Polar and high latitude substorms and solar wind conditions. Geomagn. Aeron. 54 (5), 575–582. https://doi.org/10.1134/S0016793214050041.

Despirak, I.V., Lubchich, A.A., Kleimenova, N.G., 2018. High-latitude substorm dependence on space weather conditions in solar cycle 23 and 24 (SC23 and SC24). J. Atmos. Sol. Terr. Phys. 177, 54–62. https://doi.org/10.1016/j.jastp.2017.09.011.

Despirak, I.V., Setsko, P.V., Sakharov, YaA., Lyubchich, A.A., Selivanov, V.N., Valev, D., 2022a. Observations of geomagnetic induced currents in Northwestern Russia: case studies. Geomagn. Aeron. 62 (6), 711–723. https://doi.org/10.31857/S0016794022060037 (in Russian).

Despirak, I.V., Setsko, P.V., Sakharov, YaA., Lyubchich, A.A., Selivanov, V.N., 2022b. Geomagnetic Induced Currents during Supersubstorms 7-8 September 2017. Bulletin of the Russian Academy of Sciences: Physics (accepted for publication).

Gjerloev, J.W., 2009. A global ground-based magnetometer initiative. Eos Trans. AGU 90 (27), 230–231. https://doi.org/10.1029/2009EO270002.

Hajra, R., Tsurutani, B.T., Lakhina, G.S., 2020. The complex space weather events of 2017 September. Astrophys. J. 899 (15pp), 3. https://doi.org/10.3847/1538-4357/aba2c5.

Kelly, G.S., Viljanen, A., Beggan, C.D., Thomson, A.W.P., 2017. Understanding GIC in the UK and French high-voltage transmission systems during severe magnetic storms. Space Weather 15, 99–114. https://doi.org/10.1002/2016SW001469.

Kisabeth, J.L., Rostoker, G., 1974. The expansive phase of magnetospheric substorms. I. Development of the auroral electrojets and auroral arcs configuration during substorm. J. Geophys. Res. V. 79, 972–984. https://doi.org/10.1029/JA079i007p00972.

Kleimenova, N.G., Kozyreva, O.V., Malysheva, L.M., Antonova, E.E., Kornilova, T.A., Kornilov, I.A., 2012. Wave structure of magnetic substorms at high latitudes. Geomagn. Aeron. 52, 746–754. https://doi.org/10.1134/S0016793212060059.

Kozyreva, O., Pilipenko, V., Krasnoperov, R., Baddeley, L., Sakharov, Y., Dobrovolsky, M., 2020. Fine structure of substorm and geomagnetically induced currents. Ann. Geophys. 63 (2), GM219. https://doi.org/10.4401/ag-8198.

Lakhina, G.S., Hajra, R., Tsurutani, B.T., 2020. Geomagnetically inducted current. Springer Nature Switzerland AG 2020. In: Gupta, H.K. (Ed.), Encyclopedia of Solid Earth Geophysics, Encyclopedia of Earth Sciences Series. https://doi.org/10.1007/978-3-030-10475-7_245-1.

Loomer, E.I., Gupta, J.C., 1980. Some characteristics of high latitude substorms. J. Atmos. Terr. Phys. V. 42, 645–652. https://doi.org/10.1016/0021-9169(80)90099-9.

Lui, A.T.Y., Perreault, P.D., Akasofu, S.-I., Anger, C.D., 1973. The diffuse aurora. Planet. Space Sci 21 (5), 857–861. https://doi.org/10.1016/0032-0633(73)90102-5.

Mac Manus, D.H., Rodger, C.J., Dalzell, M., Thomson, A.W.P., Clilverd, M.A., Petersen, T., Wolf, M.M., Thomson, N.R., Divett, T., 2017. Long-term geomagnetically induced current observations in New Zealand: Earth return corrections and geomagnetic field driver. Space Weather 15, 1020–1038. https://doi.org/10.1002/2017SW001635.

Newell, P.T., Gjerloev, J.W., 2011. Evaluation of SuperMAG auroral electrojet indices as indicators of substormsand auroral power. J. Geophys. Res. 116, A12211 https://doi.org/10.1029/2011JA016779.

Nosé, M., Iyemori, T., Wang, L., Hitchman, A., Matzka, J., Feller, M., Egdorf, S., Gilder, S., Kumasaka, N., Koga, K., Matsumoto, H., Koshiishi, H., Cifuentes-Nava, G., Curto, J.J., Segarra, A., Çelik, C., 2012. Wp index: a new substorm index derived from high-resolution geomagnetic field data at low latitude. Space Weather 10, S08002. https://doi.org/10.1029/2012SW000785.

Oliveira, D.M., Ngwira, C.M., 2017. Geomagnetically induced currents: principles. Braz. J. Phys. 47, 552–560. https://doi.org/10.1007/s13538-017-0523-y.

Pudovkin, M.I., Semenov, V.S., Kotikov, A.L., Shishkina, E.M., 1995. Dynamics of auroral electrojets and energetics of substorm. J. Atmos. Terr. Phys. 57, 187–192. https://doi.org/10.1016/0021-9169(93)E0033-6.

Pulkkinen, A., Lindahl, S., Viljanen, A., Pirjola, R., 2005. Geomagnetic storm of 29–31 October 2003:Geomagnetically induced currents and their relation to problems in the Swedish high-voltage power transmission system. Space Weather 3, S08C03. https://doi.org/10.1029/2004SW000123.

Sakharov, Ya A., Danilin, A.N., Ostafiichuk, R.M., 2007. Recording of GICs in power systems of the Kola Peninsula. In: Trudy 7-go Mezhdunar. Simp. Po Elektromagnitnoi Sovmestimosti I Elektromagnitnoi Ekologii (Proceedings of the 7th International Symposium on Electromagnetic Compatibility and Electromagnetic Ecology). IEEE, St. Petersburg, pp. 291–293.

Sakharov, YaA., Katkalov, YuV., Selivanov, V.N., Viljanen, A., 2016. Recording of GICs in a regional power system. In: Prakticheskie Aspekty Geliogeofiziki, Materialy Spetsial'noi Sektsii "Prakticheskie Aspekty Nauki Kosmicheskoi Pogody" 11-i Ezhegodnoi Konferentsii "Fizika Plazmy V Solnechnoi Sisteme" (Practical Aspects of Heliogeophysics: Proceedings of the Special Section "Practical Aspects of the Science of Space Weather" of the 11th Annual Conference. Physics of Plasma in the Solar System, Moscow, pp. 134–145. IKI.

Sakharov, YaA., Selivanov, V.N., Bilin, V.A., Nikolaev, V.G., 2019. Extremal values of geomagnetically inducted currents in the regional power system. Physics of Auroral Phenomena", Proc. XLII Annual Seminar, Apatity 53–56. https://doi.org/10.25702/KSC.2588-0039.2019.42.53-56 (in Russian).

Sakharov, Ya A., Yagova, N.V., Pilipenko, V.A., Selivanov, V.N., 2022. Spectral content of Pc5– 6/Pi3 geomagnetic pulsations and their efficiency in generation of geomagnetically induced currents. Russ. J. Earth Sci. 22, ES1002. https://doi.org/10.2205/2021ES000785.

Schillings, A., Palin, L., Opgenoorth, H.J., Hamrin, M., Rosenqvist, L., Gjerloev, J.W., Juusola, L., Barnes, R., 2022. Distribution and Occurrence Frequency of dB/dt Spikes during Magnetic Storms 1980–2020, vol. 20. Space Weather, e2021SW002953. https://doi.org/10.1029/2021SW002953.

Sergeev, V.A., Yahnin, A.G., 1979. Correspondence of signs of the growth phase of a substorm//Geomagnetic Research. M C J. Media Cult.: Sov. Radio. Issue 24, 78–89.

Setsko, P.V., Despirak, I.V., Sakharov, Ya A., Bilin, V.A., Selivanov, V.N., 2022. Geoinduced Currents during Supersubstorms on September 2017. September 5-10, 2022. Proceedings of the XVII Conference of Young Scientists "Interaction of fields and radiation with matter, Irkutsk, Russia, pp. 399–402. ISSN 0135-3748 (in Russian).

Tsurutani, B.T., Hajra, R., 2021. The interplanetary and magnetospheric causes of geomagnetically induced currents (GICs) > 10 A in the Mäntsälä Finland pipeline: 1999 through 2019. J. Space Weather Space Clim 11, 23. https://doi.org/10.1051/swsc/2021001.

Viljanen, A., Häkkinen, L., 1997. In: Lockwood, M., Wild, M.N., Opgenoorth, H.J.E.S.A. (Eds.), IMAGE Magnetometer Network, Satellite-Ground Based Coordination Sourcebook. publications SP, pp. 111–117, 1198. 1997.

Viljanen, A., 1998. Relation of geomagnetically induced currents and local geomagnetic feld variations. Trans Power Deliv 13, 1285–1290.

Viljanen, A., Tanskanen, E.I., Pulkkinen, A., 2006a. Relation between substorm characteristics and rapid temporal variations of the ground magnetic field. Ann. Geophys. 24 (2), 725–733. https://doi.org/10.5194/angeo-24-725-2006.

Viljanen, A., Pulkkinen, A., Pirjola, R., Pajunpaa, K., Posio, P., Koistinen, A., 2006b. Recordings of geomagnetically induced currents and a nowcasting service of the Finnish natural gas pipeline system. Space Weather 4, S10004. https://doi.org/10.1029/2006SW000234.

Vorobjev, V.G., Sakharov, YaA., Yagodkina, O.I., Petrukovich, A.A., Selivanov, V.N., 2018. Geoinduced currents and their relationship with the western electrojet position and auroral precipitation boundaries, 2018 Tr. Kol'sk. Nauchn. Tsentra Ross. Akad. Nauk 4, 16–28. https://doi.org/10.25702/KSC.2307-5252.2018.9.5.16-28.

Watari, S., Nakamura, S., Ebihara, Y., 2021. Measurement of geomagnetically induced current (GIC) around Tokyo, Japan, 2021 Earth Planets Space 73, 102. https://doi.org/10.1186/s40623-021-01422-3.

Wiens, R.G., Rostoker, G., 1975. Characteristics of the development of the westward electrojet during the expansive phase of magnetospheric substorms. J. Geophys. Res. 16, 2109–2128. https://doi.org/10.1029/JA080i016p02109.

Yagova, N.V., Pilipenko, V.A., Sakharov, YaA., Selivanov, V.N., 2021. Spatial scale of geomagnetic Pc5/Pi3 pulsations as a factor of their efciency in generation of geomagnetically induced currents. Earth Planets Space 73, 88. https://doi.org/10.1186/s40623-021-01407-2.

Yahnin, A.G., Sergeev, V.A., Pellinen, R.J., Baumjohann, W., Kaila, K.U., Ranta, H., Kangas, J., Raspopov, O.M., 1983. Substorm time sequence and microstructure on 11 November 1976. J. Geophysics - Zeitschrift für Geophysik. 53 (3), 182–197.

Yao, Z., Rae, I.J., Lui, A.V.T., Murphy, K.R., Owen, C.J., Pu, Z.Y., Forsyth, C., Grodent, D., Zong, Q.-G., Du, A.M., Kalmoni, N.M.E., 2017. An explanation of auroral intensification during the substorm expansion phase. J. Geophys. Res. Space Physics 122, 8560–8576. https://doi.org/10.1002/2017JA024029.

Yermolaev, YuI., Nikolaeva, N.S., Lodkina, I.G., Yermolaev, M.Yu, 2009. Catalog of large-scale solar wind phenomena during 1976–2000. Cosmic Res. 47 (2), 81–94.